Desalination and Water Treatment
www.deswater.com

doi: 10.5004/dwt.2023.29346

287 (2023) 46–58
March

Green technique of visible light active titanium dioxide nanoparticles using starch for the degradation of organic pollutant

Nornadia Nazuha Abu Hasim[a], Nurul Hidayah Mohamad Idris[a], Hairul Hisham Hamzah[b], Georg Urstöger[c], Benedikt Schrode[c], Hooi Ling Lee[a,*]

[a]*Nanomaterials Research Group, School of Chemical Sciences, Universiti Sains Malaysia, 11800 USM, Penang, Malaysia, emails: hllee@usm.my (H.L. Lee), dhuhanan@gmail.com (N.N.A. Hasim), hidayahidris@student.usm.my (N.H.M. Idris)*
[b]*School of Chemical Sciences, Universiti Sains Malaysia, 11800 USM, Penang, Malaysia, email: hishamhamzah@usm.my (H.H. Hamzah)*
[c]*Anton Paar GmbH, Anton-Paar-Stra β e 20, 8054 Graz, Austria, emails: georg.urstoeger@anton-paar.com (G. Urstöger), benedikt.schrode@anton-paar.com (B. Schrode)*

Received 31 October 2022; Accepted 5 February 2023

ABSTRACT

The design of titanium dioxide nanoparticles (TiO_2 NPs) is crucial. Therefore, the visible light-activated TiO_2 NPs were proposed using a sol–gel green method with reduced optical bandgap energy from 3.20 eV of pure anatase TiO_2 into 3.00 eV. The obtained electrochemical bandgap (2.81 eV) which was analyzed by cyclic voltammetry revealed an insignificant difference compared to the optical bandgap. X-ray diffraction analysis verified TiO_2 NPs composed of an anatase-brookite phase with a crystallite size of 8 nm. The particle size of TiO_2 NPs was confirmed by high-resolution transmission electron microscopy analysis (11.63 ± 1.47 nm). Due to the high photocatalytic performance of the mixed-phase TiO_2 NPs, the optimum concentration (6 ppm) of neutral red (NR) dye was completely degraded within 30 min under visible light. Photoluminescence analysis revealed the improved electron–hole separation of the synthesized TiO_2 NPs. $^{\bullet}O_2^-$ acted as the predominant role of reactive oxygen species in the removal of NR dye. The degradation kinetics of NR obeyed the first-order kinetic and the adsorption data were fitted with the Langmuir isotherm model. TiO_2 NPs maintained over 90% of its initial photocatalytic efficiency after five cycles. Thus, this study suggests that the TiO_2 NPs have good potential as an effective photocatalyst in wastewater treatment.

Keywords: Titanium dioxide nanoparticles; Visible light; Starch; Green synthesis; Wastewater treatment

1. Introduction

Rapid industrial development and urbanization have resulted in a massive generation of industrial and domestic wastewater which led to serious contamination in many countries worldwide. According to the World Bank, textile dyeing is estimated to be responsible for 17%–20% of industrial water pollution. Generally, most dyes are toxic and potentially carcinogenic and their removal from the industrial effluents is a major environmental problem [1]. Considering the problem, it is critical to develop well-organized strategies for effective wastewater decontamination. Different methods such as photocatalysis, absorption, ion exchange, and filtration have been suggested to eliminate pollutants from wastewater [2–5]. Among these methods, photocatalysis that utilizes semiconductors has emerged as a promising and advanced environmental nanotechnology [6].

* Corresponding author.

In 1929, there was a significant breakthrough in photocatalysis due to discovery titanium dioxide (TiO_2) as a photocatalyst [7]. Titanium dioxide is an *n*-type semiconductor metal oxide that possesses excellent chemical stability, easy operation with low cost and intriguing electrochemical properties and; has excellent magnetic and catalytic properties [8,9]. Photocatalytic reactions of TiO_2 for degrading organic pollutants are based on light energy absorption and photo-generated electron transfer in the bandgap of TiO_2 [10]. However, anatase TiO_2 has a wide bandgap of ~ 3.2 eV with a wavelength that is under ultraviolet radiation (~400 nm) [11]. Anatase TiO_2 usually utilizes ultraviolet light (UV), which accounts for only 5% of sunlight. It has restricted the practical application of this oxide as it could not operate another 45% of visible light in solar radiation [11]. Moreover, the quick recombination of electron–hole pairs is also a significant limitation in photocatalysis [12]. Electron–hole recombination occurring at faster rates is not favorable in a photocatalytic reaction as it gives insufficient time for critical chemical reactions to occur [13]. The electrons and holes that successfully travel to the semiconductor's surface without recombining can be involved in the reduction and oxidation reactions, which are the foundations for organic pollutant photodegradation in wastewater decontamination [14]. Thus, to mitigate the drawbacks, creating visible light-active TiO_2 photocatalysts that can employ both UV and visible radiation in the solar spectrum as well as a slower recombination rate, is of major interest.

Many attempts have been employed to synthesize useful TiO_2 photocatalysts. In our previous work, significant effort has been made by Muniandy et al. [15]; they have successfully synthesized TiO_2 nanoparticles (NPs) using the green chemistry sol–gel method [15]. Whereas the latest of our work has employed a similar approach that developed a TiO_2/PVA/cork floating photocatalyst to alleviate the disadvantages of the suspended TiO_2 photocatalysis system [16]. The observations revealed that the recombination rate of synthesized TiO_2 NPs has been slower due to the presence of Ti^{3+} ions in the TiO_2 NPs. The Ti^{3+} ions act as electron traps which inhibit the recombination of electrons and holes [16]. Additionally, both mentioned studies show a smaller bandgap of TiO_2 NPs (3.0 eV) and have good photodegradation under visible light irradiation. This justification was also supported by Yang et al. [17]. They found that the sol–gel technique that has transformed the Ti^{4+} to Ti^{3+} ions can facilitate the separation of photogenerated electrons and holes. It ensures that the h^+ has more chance to participate in the oxidization or turn into a more powerful oxidant $^{\bullet}OH$ in photocatalysis. Therefore, the sol–gel method has been recognized to contribute significantly to the production of visible light active TiO_2 photocatalysts with a slower electron–hole recombination rate. This high-potential TiO_2 photocatalyst is effective for the removal of contaminants in water. Thus, the current studies of based-TiO_2 photocatalysts using this method have been summarized in Table 1.

Recently, many researchers have used neutral red (NR) as substitute for dyes pollutants to test photocatalysts' performance in wastewater treatment. NR is one of the basic dyes from the azine series, belonging to the quinone-imine dyes class [18]. Johnsen et al. [19] revealed the properties of NR such as resistance to nucleophilic degradation, low water solubility and high solid–water distribution ratio. Several studies have documented the NR's photocatalytic degradation and toxicity reduction using various catalysts such as TiO_2 nanocatalyst, ZnO photocatalyst, Fe_3O_4 nanospheres and BiOCl photocatalyst [18,20–22]. According to Sarwan et al. [22], neutral red molecules interact with $^{\bullet}O_2^-$, $^{\bullet}HO_2$ radicals or $^{\bullet}OH$ species to produce intermediates and subsequently form the degradation product. The adsorbed dye molecule traps the hole on the catalyst surface, creating a reactive radical state that may decay due to recombination with an electron [23]. Hence, the study of the degradation of neutral red is essential in determining the prepared photocatalyst's degradation performances.

In this study, TiO_2 nanoparticles were synthesized using the green sol–gel technique. The photocatalyst was produced using a solvent-free precipitation process with soluble starch as a template agent and titanium tetraisopropoxide (TTIP) as a precursor under lower temperatures (below 200°C). As such, this technique could decrease the use of hazardous substances towards humans and the environment. Subsequently, this method has been recognized as a green technique to produce visible light active TiO_2 photocatalysts with a slower electron–hole recombination rate to remove contaminants in water. Furthermore, this sol–gel approach has advantages such as operating at low temperatures and regulating synthesized nanoparticles' morphology and particle size is possible [24]. Additionally, the soluble starch applied as a templating agent has unique traits including large specific surface area, large pore volume, enhanced active sites, good adsorption ability, and mechanical stability [25]. These excellent features contribute to the good photocatalytic performance of the synthesized TiO_2 NPs. Both our previous studies have successfully investigated methylene blue as a model pollutant, whereby was known

Table 1
Studies of based-TiO_2 photocatalyst using the sol–gel method

No.	Catalyst	Bandgap energy of catalyst (eV)	Photocatalytic activity	References
1	TiO_2	3.00	100.00% of methylene blue removal for 30 min	[15]
2	TiO_2	3.20	80.89% of methylene blue removal for 60 min	[26]
3	TiO_2/cork	3.00	98.43% of methylene blue removal for 120 min	[16]
4	Ag-TiO_2	2.67	97.00% of methylene blue removal for 35 min	[27]
5	Fe-TiO_2	2.86	97.31% of methylene blue removal for 150 min	[28]
6	TiO_2	3.00	85.00% of methylene blue removal for 240 min	[29]

as a cationic dye. The findings proved that the synthesized TiO_2 NPs have excellent photocatalytic performance for methylene blue removal. To explore the robustness of different types of dyes, the neutral red dye, known as a neutral dye, was selected as a model pollutant in this study. Hence, the photocatalytic performance of synthesized TiO_2 NPs was further investigated for a neutral dye in this research.

2. Experimental section

2.1. Materials

Titanium(IV) isopropoxide (TTIP, ≥ 97%) was obtained from Sigma-Aldrich, Co., USA. Soluble starch was purchased from System Laboratory Chemicals & Reagents, Malaysia. Ammonia solution (NH_4OH) was purchased from Merck KGaA Analyticals, EMD Millipore, Co., Germany. Potassium chloride (KCl, >99%) was acquired from Fisher Scientific, Malaysia. Methanol (MeOH) and ethanol (C_2H_5OH); acetonitrile (ACN), silver nitrate ($AgNO_3$), sodium pyruvate ($C_3H_3NaO_3$), ascorbic acid ($C_6H_8O_6$) were obtained from Sigma-Aldrich, Co., USA and NR were purchased from QREC, Grade AR, (Asia) Sdn. Bhd., Malaysia. All reagents were used as purchased and without further purification.

2.2. Synthesis of TiO_2 nanoparticles (TiO_2 NPs) by sol–gel method

TiO_2 NPs were synthesized based on a previous study by Muniandy et al. [15]. First, 5.0 g of soluble starch was dissolved in 150 mL boiling distilled water with 0.01 mol of TTIP added to the starch solution and mixed homogeneously at 85°C for 5 min. The mixture was then stirred for 30 min after the pH of the solution was maintained at pH 9 by adding ammonia solution (NH_4OH). Next, the white precipitate formation was centrifuged at 8,500 rpm for 10 min, followed by 5 washing cycles with distilled water. After that, it was dried in an oven at 50°C. Lastly, the white powder obtained was calcined at 500°C for 2 h in the furnace to obtain nanoparticles of TiO_2.

2.3. Evaluation of photocatalytic activities

The photocatalytic oxidation of NR under sunlight irradiation was performed to evaluate the photocatalytic activities of the synthesized TiO_2 NPs. The study dispersed 0.1 g of the synthesized TiO_2 NPs in 200 mL of NR solution. The mixture was stirred in the dark for an hour to reach adsorption equilibrium and transferred to an open area under bright sunlight (luminosity between 80–100 kLux). The samples were collected at a regular time interval of 10 min for 2 h with a nylon syringe filter (Ø = 25 mm, pore diameter 0.22 μm). The samples taken were immediately analyzed by LAMBDA 25 UV-Visible spectrophotometer. In this study, three initial dye concentrations of NR, namely 6, 8, and 10 ppm were used to determine the optimized conditions for degradation of neutral red under sunlight irradiation. The removal efficiency of NR solution can be calculated using the following Eq. (1):

$$R = \frac{C_0 - C_t}{C_0} \times 100\% \quad (1)$$

where C_0 is the initial concentration of NR and C_t is the concentration of the NR at respective time intervals.

2.4. Adsorption isotherm studies

Adsorption experiments were carried out under dark conditions for an hour by mixing 0.1 g of photocatalyst sample with 200 mL of NR solution. The initial concentration of NR solutes, C_0, used in this study was 6, 8, and 10 ppm. The sample was taken every 10 min until the solution reached equilibrium. The equilibrium of the solution was determined using a LAMBDA 25 UV-Visible spectrophotometer (wavelength λ = 530 nm). Subsequently, the concentration at equilibrium, C_e was recorded. The amounts of neutral red adsorbed that should be adsorbed were calculated from the concentrations in solutions before and after adsorption.

2.5. Mineralization studies

The degree of mineralization for neutral red treated with a synthesized sample was determined using a total organic carbon (TOC) analyzer (Shimadzu, TOC-L, Japan). The aliquots of the sample taken from treating the neutral red (NR) under sunlight were filtered and injected into the system using a 0.45 μm nylon membrane filter. All carbon forms in the sample were transformed to CO_2, which was then measured directly or indirectly and converted to total organic carbon or total carbon content based on the presence of inorganic carbonates.

2.6. Scavenging study

The scavenging test was carried out to investigate the reactive radical species that played a prominent role in the photocatalytic degradation of NR. The reaction was carried out in a protocol similar to the photocatalytic experiment (Section 2.3 – Evaluation of photocatalytic activities) but with the presence of different radical scavengers such as methanol (10% v/v of MeOH), silver nitrate (0.2 M of $AgNO_3$), acetonitrile (100% v/v of ACN), sodium pyruvate (0.2 M of $C_3H_3NaO_3$) and ascorbic acid (0.2 M of $C_6H_8O_6$). Methanol, silver nitrate, acetonitrile, sodium pyruvate, and ascorbic acid were used as scavengers for the photogenerated holes (h^+), superoxide radicals ($^{\bullet}O_2^-$), hydroxyl radicals ($^{\bullet}OH$), hydrogen peroxide (H_2O_2) and singlet oxygen ($^1O_2$), respectively [16,29–32].

2.7. Reusability study of TiO_2 NPs

The reusability of TiO_2 nanoparticles was tested in a total of five cycles in duplicates. The sample taken from each photocatalytic reaction under sunlight was washed for 15 min in boiling distilled water. The sample was then dried overnight in the oven at 100°C. The photocatalyst could be treated under the same conditions to be recycled for the next photocatalytic reaction.

2.8. Characterizations

Crystallite size and crystalline phase of the synthesized photocatalyst were analyzed by powder X-ray diffractometer

(XRDynamic 500; Anton Paar, Austria) equipped with a Primux 3000 sealed-tube X-ray source with copper anode and a goniometer radius of 400 mm using Cu K_α (1.541 Å) radiation in the range 2θ = 15°–105°. Data analysis was performed using the X-ray diffraction (XRD) analysis PRO (Anton Paar, Austria) software package. The XRD analysis was carried out in the XRD laboratory of Anton Paar GmbH, Austria. The morphology and the size of TiO_2 NPs were characterized by the high-resolution transmission electron microscopy (HRTEM) technique using a high-resolution transmission electron microscope (FEI Tecnai G^2 20 S-TWIN, Spain). The suspension was obtained when TiO_2 NPs (10 mg) were dispersed in 10 mL of ethanol, followed by sonication. Then, a few drops of the suspension were dried on the 200-mesh carbon-coated copper grids for HRTEM analysis. The size and shape of the particles were analyzed at an acceleration voltage of 300 kV and imaged at low and high magnification. All the obtained HRTEM images were analyzed by using the open software ImageJ (ImageJ 1.51j8, USA). Fourier-transform infrared (FTIR) spectra of the prepared powders were measured by the KBr pellet method in the range of 400–4,000 cm^{-1} using a PerkinElmer System 2000 spectrophotometer (USA). Ultraviolet-visible (UV-Vis) diffuse reflectance spectra (DRS) were employed to measure the bandgap changes and shifting of wavelength in the synthesized material. The measured spectra were recorded on PerkinElmer Lambda 35 Spectrometer (USA) equipped with the diffuse reflectance standard and Labsphere RSAPE-20 integration sphere. The electrochemical (EC) bandgap of TiO_2 NPs was analyzed using the modified glassy carbon (GC) electrode surfaces which were left for 30 min to make them dry to obtain TiO_2 modified GC electrodes. The modified electrodes were then measured in a 0.1 M KCl solution to monitor the coated TiO_2 as an electrocatalyst for hydrogen evolution reaction (HER) and oxygen evolution reaction (OER), respectively, using a cyclic voltammetric technique at a scan rate of 100 mV/s. During the measurement, nitrogen (N_2) gas was kept purging in an electrochemical cell to remove the dissolved oxygen in the KCl solution entirely. Further analysis was conducted using PerkinElmer LS 55 Luminescence Spectrometer (USA) with a laser excitation wavelength of 325 nm and an acquisition time of 10 s to study the transfer and recombination process of charge carriers.

3. Results and discussion

3.1. XRD and HRTEM analyses

In order to identify the crystalline structure and phases of the TiO_2 NPs, an XRD analysis was conducted in this study. On the other hand, HRTEM analysis determines the size, shape, and size distribution of TiO_2 NPs. Fig. 1 depicts the XRD pattern of the synthesized TiO_2 NPs sample. Broad Bragg peaks confirm the presence of nanocrystalline material. The peaks could be ascribed to the tetragonal anatase phase (PDF 04-006-1918) and the orthorhombic brookite phase (PDF 00-015-0875). The anatase-brookite ratio was measured by the Rietveld refinement method, resulting in a composition of 84% (anatase) and 16% (brookite). The obtained diffraction peaks were found at 2θ values 25.33°, 37.92°, 48.03°, 54.58°, 62.74°, 69.22°, 70.09°, 75.28°, and 82.79°, respectively, corresponding to the diffraction planes (101), (004), (200), (105), (211), (204), (116), (215), and (303) of anatase TiO_2 [15,33,34]. Moreover, it should be noted that the overlapping of the main anatase reflection (101) with the brookite reflections of (120) and (111) was hardly noticeable in the XRD pattern, due to the broad peaks [35]. As such, the presence of the brookite phase was determined at 2θ = 29.61°, which was assigned to the brookite (121) crystal plane. In previous studies on the synthesized anatase-brookite phase photocatalysts *via* the simple hydrolysis of titanium isopropoxide, the formation of brookite when calcined at temperatures below 500°C has been reported [36]. This fact was consistent with this study, whereby the anatase-brookite phase was achieved by calcining the TiO_2 NPs at 500°C through the sol–gel method using titanium isopropoxide as a precursor. Additionally, it was reported that the anatase-brookite mixture of crystalline phase TiO_2 NPs exhibited higher photocatalytic activity than the anatase phase of TiO_2 [37]. Furthermore, the anatase-brookite of TiO_2 NPs was synthesized at low temperatures which are in good agreement with Kandiel et al. [38]. Although the method was employed at low temperatures, the prepared anatase-brookite of TiO_2 NPs showed an excellent result in the removal of pollutants. Simultaneously, this allows a reduction in production costs.

A sharp and more intense peak obtained from the synthesized TiO_2 NPs was contributed by the calcination process that increases the crystallinity of nanoparticles [15]. As a result, the amorphous phase of TiO_2 was transformed into a higher crystalline phase, which was reported to boost photocatalytic activity [39]. Furthermore, the average crystallite size has become larger as seen by the reduction in the full width at half maximum intensity (FWHM) of the diffraction peak [15]. Scherrer's formula Eq. (2) was used to calculate the crystallite sizes (*D*) based on the FWHM.

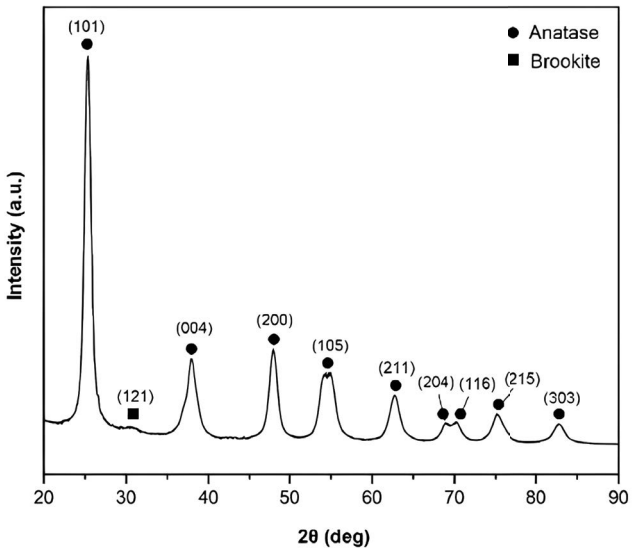

Fig. 1. XRD pattern of the synthesized TiO_2 NPs. The Miller indices of the reflections are marked (anatase phase: PDF 04-006-1918 and brookite phase: PDF 00-015-0875).

$$\tau = \frac{K\lambda}{(\beta\cos\theta)} \quad (2)$$

where τ is the average crystallite size of the solid particle, K is the Scherrer constant (0.9), λ is the X-ray wavelength (0.154 nm), and β is the FWHM. The most intense reflection is at the main anatase reflection (101), 2θ = 25.33° as shown in Fig. 1. Therefore, the τ value of the synthesized TiO_2 NPs is found to be 8 nm. However, the result demonstrates that the crystallite size of the synthesized TiO_2 NPs is less than pure anatase TiO_2 (12.96 nm) [40]. In addition, the peak broadening in the XRD profile confirms that TiO_2 NPs consist of small particles as reflected in the pattern.

The particle size of TiO_2 NPs was analyzed from HRTEM images in Fig. 2a and b, displaying the particles were in irregular spherical structures and the shadow region demonstrated that the nanoparticles have agglomerated. The particle size distribution achieved was from 9 to 16 nm, with a particle size average of 11.63 ± 1.47 nm as shown in Fig. 2d. Furthermore, the high magnification image in Fig. 2c revealed the interplanar distance of TiO_2 NPs from the lattice fringes corresponded to 0.35 nm of the anatase phase (101) [40]. The lattice parameter was measured from the fast Fourier transform image of the selected area, as depicted in the inset of Fig. 2c. However, it is significant to highlight that even though several micrographs were obtained, it was difficult to distinguish the presence of brookite nanoparticles due to the low composition of brookite in TiO_2 NPs. This observation was consistent with the small crystallite size of TiO_2 NPs as calculated from the XRD result. Therefore, this finding verified that the small particles of the synthesized TiO_2 NPs have a larger surface area than pure anatase TiO_2 [27]. Thus, the small particle size of the catalysts is one of the vital factors affecting the photodegradation of pollutants. This strategy has been accomplished by increasing the surface area of the catalyst, whereby it was expected to provide more active sites.

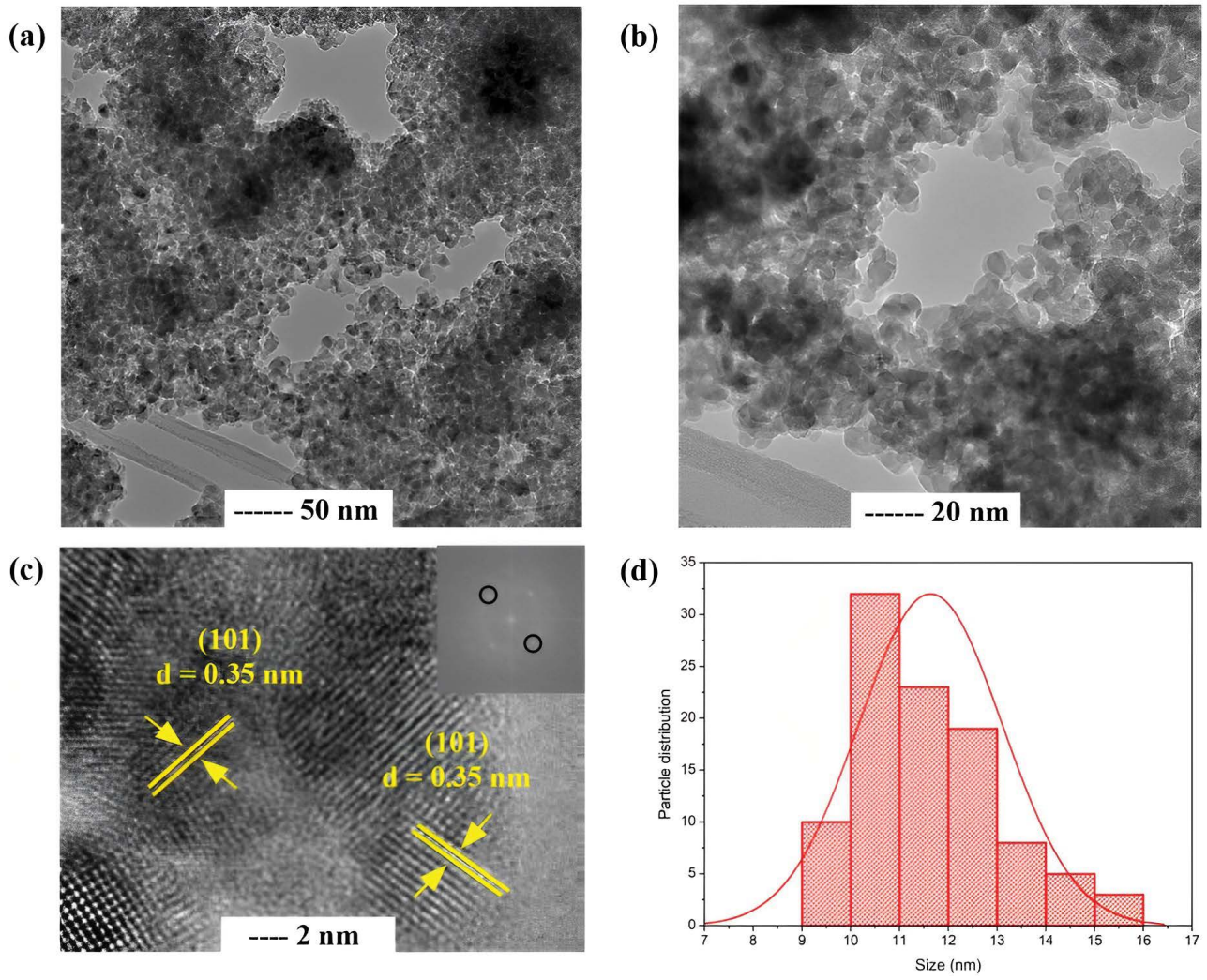

Fig. 2. (a–c) High-resolution transmission electron microscopy images of TiO_2 NPs with high and low magnifications. The inset in (c) shows fast Fourier transform image corresponding to the selected area and (d) particle size distribution of TiO_2 NPs.

Subsequently, this would improve the photocatalytic performance of the prepared catalyst [41].

3.2. FTIR analysis

The FTIR analysis was carried out to get insight into the chemical composition of the synthesized TiO_2. FTIR spectrum of the TiO_2 NPs is illustrated in Fig. 3. From the figure, the broadband between 3,500 and 2,400 cm^{-1} was attributed to the stretching of OH bending of TiO_2 NPs in the FTIR spectrum [16]. This spectrum can be referred to as the existence of a hydroxyl group on the oxide surfaces with stretching and bending modes of vibrations from physically adsorbed water. The bending of Ti–OH was observed at 1,627 cm^{-1} peak, indicating adsorbed water, while the peak at 1,452 cm^{-1} corresponds to the Ti–O modes' stretching vibrations and appeared as a weak peak. In addition, C–O bonding was noticed around 1,048 cm^{-1} due to the utilization of titanium precursor (TTIP) during the synthesis of TiO_2 NPs. The presence of Ti–O–Ti bonds was further confirmed with the occurrence of a peak at 688 cm^{-1}. Moreover, the broad bands in the range of 400–800 cm^{-1} indicated the existence of crystalline TiO_2 [36]. Thus, the presence of these functional groups in the FTIR spectrum confirmed the successful synthesis of TiO_2 NPs by the green approach.

3.3. Bandgap energy analysis

The bandgap energy of obtained TiO_2 NPs was determined using two different measurements including UV-Vis DRS and cyclic voltammetry (CV). From the measurement of UV-Vis DRS, Fig. 4 demonstrates the optical bandgap energy by extrapolating the linear region from the graph of $(ahv)^2$ vs. photon energy throughout the wavelength range of 200–800 nm. The optical bandgap energy was evaluated using Kubelka–Munk's theory [37]. The bandgap spectrum of TiO_2 NPs is shown in the inset of Fig. 4. Maximum absorbance was observed at 407 nm which corresponds to a bandgap of 3.0 eV. It shows that the bandgap has reduced to 3.0 from 3.2 eV of pure anatase in TiO_2 NPs. The reduction of bandgap could be due to the employment of basic pH solution since TiO_2 NPs were synthesized through the sol–gel technique with 0.01 mol concentration of TTIP of basic pH solution (pH 9). Moreover, our previous X-ray photoelectron spectroscopy study observed that the surface defects of Ti^{3+} ions played a significant role as they are active sites for oxygen adsorption and for trapping electrons to prevent the recombination of electrons and holes [15]. Additionally, the localized gap states induced by the self-doping of Ti^{3+} ions and oxygen vacancies might also contribute to the reduced bandgap of synthesized TiO_2 [15]. The Ti^{3+} surface defects are created by the reduction of Ti^{4+} ions which are caused by the loss of oxygen atoms in a reductive treatment or from the electron trapping under UV radiation. Meanwhile, the occupancy of oxygen vacancies can increase the donor density, promoting the separation of electron–hole pairs [42]. Hence, these surface defects are crucial in enhancing the optical properties of the catalyst.

To validate the findings of optical bandgap, the electrochemical bandgap of synthesized TiO_2 NPs was analyzed from the CV measurement for comparison. CV provides direct information on the reduction and oxidation potentials of the photocatalyst. Fig. 5a and b show cyclic voltammograms of bare and TiO_2 modified GC electrodes in a 0.1 M KCl solution, respectively. Two different potential scans were carried out on the bare GC and TiO_2 modified GC electrodes. Fig. 5a shows CV measurements were made from 0 to –2.0 V to monitor HER. It can be seen that when measured bare GC electrode in a purged of KCl solution, a flat CV response was obtained. In contrast, for the TiO_2-modified GC electrode, shows that a significant cathodic peak at ~ –1.7 V vs. SCE appeared and was designated as C_1. This dictates that the coated TiO_2 provides an excellent electrocatalyst platform for HER. Fig. 5b shows that the CV measurements were scanned from 0 to 1.2 V.

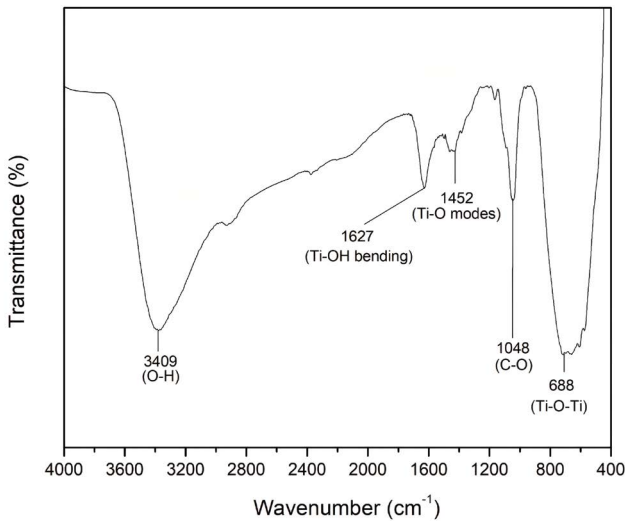

Fig. 3. Fourier-transform infrared spectrum of synthesized TiO_2 NPs.

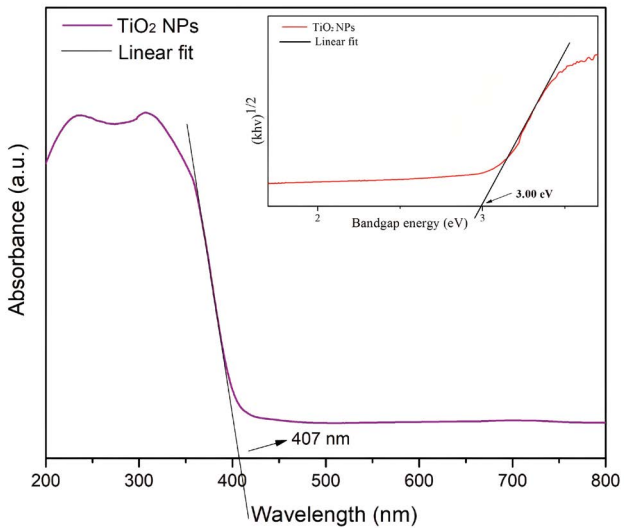

Fig. 4. UV-Vis absorption of synthesized TiO_2 NPs with inset shows the optical bandgap spectrum of TiO_2 NPs.

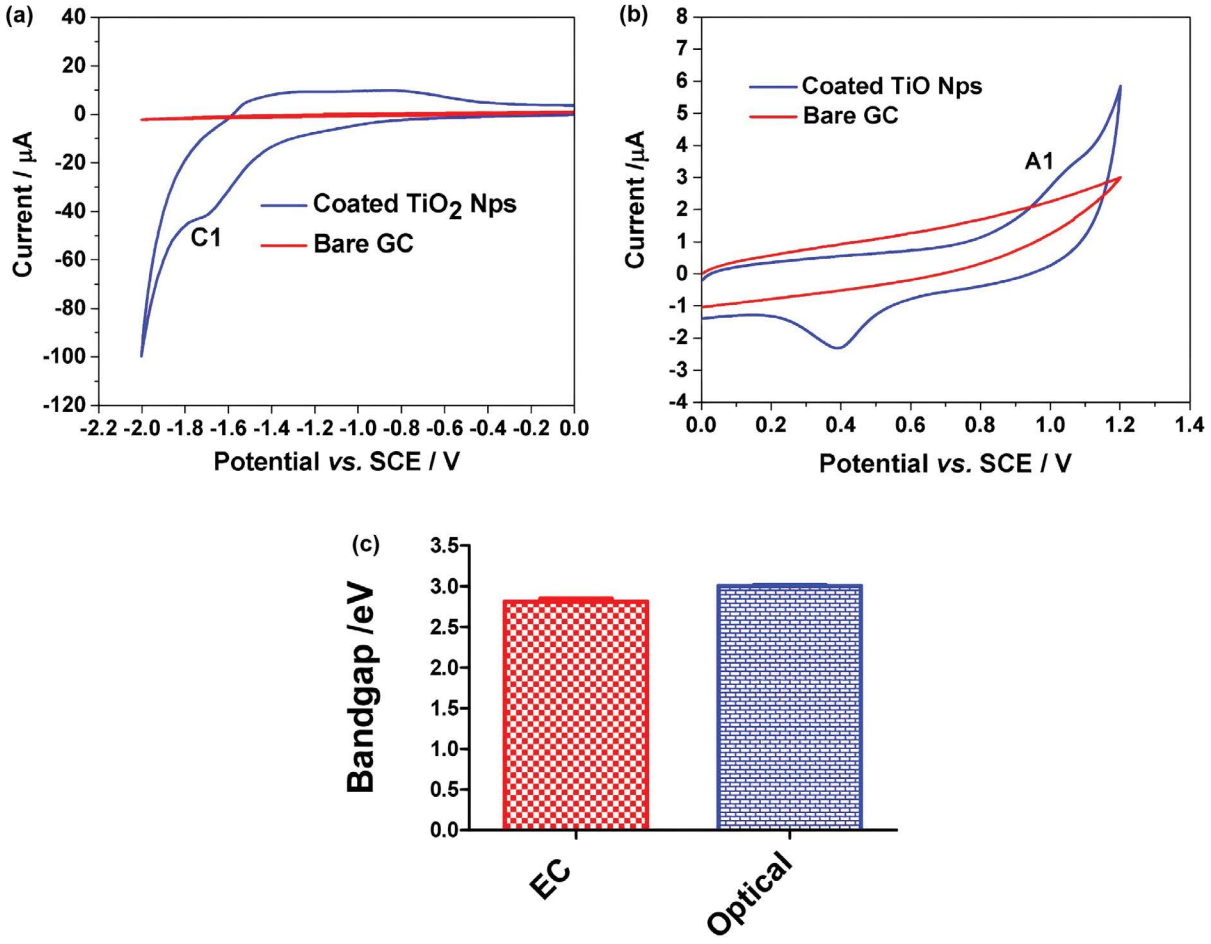

Fig. 5. Cyclic voltammograms for bare GC and TiO_2 modified GC electrodes in a 0.1 M KCl solution at a scan rate of 100 mV/s. (The geometrical electrode surface area is 0.071 cm^2): (a) cyclic voltammetry measurements were scanned from 0 to –2.0 V vs. SCE, (b) cyclic voltammetry measurements were scanned from 0 to 2.0 V vs. SCE, and (c) bar graph for comparing electrochemical bandgap with optical bandgap (n = 3).

The CV response for the coated electrode demonstrates that an anodic peak was considerably seen at ~ 1.1 V vs. SCE, indicating that the OER occurred at the coated TiO_2 NPs and, denoted as A_1. By following an approach as reported by Haram et al. [43], the bandgap of the coated TiO_2 NPs is calculated based on peak separation between A_1 and C_1, as shown in Eq. (3), whereby E_{pa} and E_{pc} represent the anodic peak potential and the cathodic peak potential, respectively:

$$\text{Bandgap} = E_{pa} \text{ for } A1 - E_{pc} \text{ for } C1 \quad (3)$$

This is because the redox potential peak separation between A_1 and C_1 can be connected directly to the electron transfer between the highest occupied molecular orbital (HOMO) and lowest occupied molecular orbital (LOMO) of the electrode reactions from the coated TiO_2 NPs at the GC electrode [43,44]. Therefore, the bandgap of the coated TiO_2 NPs via CV measurements was found to be 2.81 eV. In essence, the difference between the optical and electrochemical bandgap is considered in the range of ~ 0.2–0.4 eV as a good outcome [43]. As such, this observation verified that the EC bandgap is a statistically not significant difference as compared to the optical bandgap based on the student's t-test as displayed in Fig. 5c. This signifies that the coated TiO_2 NPs on the GC electrode surfaces exhibit excellent electrocatalytic activities due to the lower overpotential required for HER and OER [43,44]. Furthermore, the difference in the bandgap values between the two techniques can be attributed to the other effects such as solvation, reference electrode used, electrode materials employed, and electrode surface morphologies during the CV procedure. Hence, both above-mentioned bandgap measurements demonstrated that the synthesized TiO_2 NPs can utilize the visible light spectrum during the photocatalytic process with a reduced bandgap of the photocatalyst.

3.4. Photoluminescence analysis

The photoluminescence (PL) spectra of the pure anatase TiO_2 and the TiO_2 NPs are presented in Fig. 6 to give information regarding the transfer behavior of the electron–hole pairs under a laser excitation wavelength of

325 nm and an acquisition time of 10 s. It was discovered that there was broad emission in the spectral range from 350 to 500 nm, as well as the presence of well-resolved peaks and shoulders. The synthesized TiO_2 NPs and pure anatase TiO_2 particles are emissive, with well-resolved PL spectra extending into visible spectral regions due to the existence of oxygen vacancies [35]. Based on Fig. 6, synthesized TiO_2 NPs have lower intensity compared to the pure anatase TiO_2. This is attributed to the slower rate of recombination of photo-induced electron–hole pairs of TiO_2 NPs compared to pure anatase TiO_2 [14]. Furthermore, it may be the presence of Ti^{3+} ions as electron traps in the TiO_2 NPs enhance the lifetime of the charges [15]. In the previous study, Plešngerová et al. [45] discovered that the oxygen vacancies acted as the recombination centers, which the photogenerated carrier lifetime of the catalyst could be longer with increasing oxygen vacancy concentration. Subsequently, the photocatalytic performance of TiO_2 NPs was elevated. Meanwhile, the electron–hole recombination occurring at a faster rate is unfavorable in a photocatalytic reaction because it provides insufficient time for specific chemical reactions [13]. Thus, photocatalysts with lower PL intensity exhibited higher photocatalytic efficiency [37].

3.5. Photocatalytic activity and kinetic studies of TiO_2 NPs

3.5.1. Effect of initial dye concentration on the photocatalytic activity of TiO_2 NPs

The ability of TiO_2 NPs as a photocatalyst in photocatalytic degradation of neutral red (NR) was examined under sunlight irradiation. Neutral red (NR) was selected as a model dye in wastewater since it was one of the hazardous organic neutral dyes which exist in the wastewater and cause serious environmental problems [38]. In this experiment, the degradation efficiency of NR solution was studied with different initial dye concentrations (6, 8 and 10 ppm), as shown in Fig. 7a. The objective of this experiment was to ascertain the optimal dye concentration for degradation of neutral red under sunlight irradiation with other conditions kept constant. The result shows the degradation of NR with 6 ppm dye concentration achieved the fastest complete degradation at 30 min with the solution's color shifted from red to colorless. Meanwhile, for 8 and 10 ppm of dye concentration, the time to achieve complete degradation efficiency was 80 and 100 min, respectively. Hence, the result shows that further increased dye concentration will decrease the photocatalytic activity of the TiO_2 NPs.

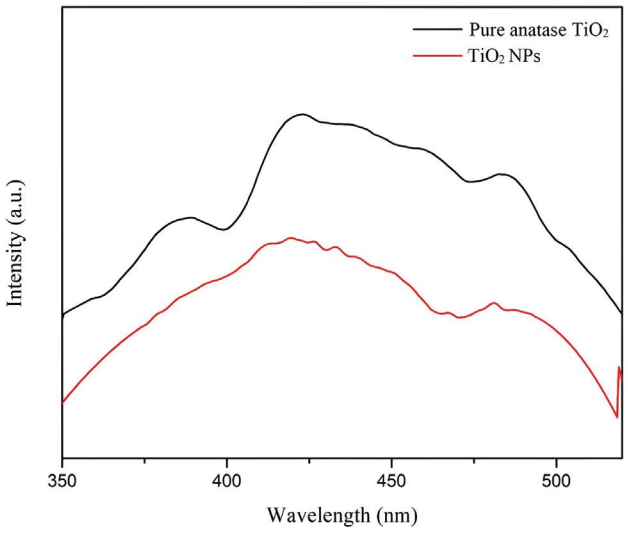

Fig. 6. PL spectra of the synthesized TiO_2 NPs and pure anatase TiO_2.

The dye concentration at 10 ppm showed the lowest photocatalytic efficiency due to increased dye concentration. The increase in dye concentration with decreasing the rate of the reaction could cause by the quick action of the dye molecules to occupy the active sites at TiO_2's photocatalyst surface and photons' penetration has been severely reduced through the dye [46]. Penetration of photons is substantial in photocatalytic activity as it can induce a reaction and perform complete mineralization from the existence of active species on TiO_2 NPs' surface. Furthermore, increasing dye concentration beyond optimal conditions can cause the reaction to slow down due to the number of dye molecule collisions increasing while dye molecule collisions with $^{\bullet}OH$ radicals decrease [47]. This finding was consistent with Hanafi and Sapawe [48], whereby they investigated the lower degradation of Remazol Brilliant Blue dye reached at a higher concentration of the dye. This was due to the creation of several layers of adsorbed dye molecule on the surface of the catalyst, causing no direct contact of light to produce hydroxyl radicals. Consequently, this circumstance would inhibit the photoreaction to occur.

The graph of the first-order kinetic model was employed for the kinetic analysis of photocatalytic degradation of NR as shown in Fig. 7b. The slopes of linear plots $\ln(C_0/C_t)$ vs. time were used to calculate the rate constants (k). The result for rate constants, k obtained was consistent with the results obtained from the photodegradation, which were 0.1643, 0.0458 and 0.0364 min^{-1} for initial dye concentration at 6, 8 and 10 ppm, respectively, as tabulated in Table 2. It demonstrates that the reaction rates increase as the dye concentration decreases. Next, the correlation coefficient (R^2) can be determined from a first-order linear graph, as shown in Fig. 7b. The correlation coefficient obtained was the highest for 6 ppm concentration (0.9831) followed by 8 ppm concentration (0.9580) and 10 ppm concentration (0.9433). Hence, the result shows the photocatalytic activity worked best at 6 ppm dye concentration with both rates constant and the correlation coefficient is the highest compared to other dye concentrations.

3.6. Adsorption isotherm studies

Adsorption isotherm studies were conducted in the dark to determine the TiO_2 NPs' adsorption capability as well as their interactions with dye molecules. The dispersion of TiO_2 nanoparticles is represented by the isothermal models of Langmuir and Freundlich. The adsorption isotherm curves based on Langmuir and Freundlich isotherms are plotted in Fig. 8a and b, respectively. For the Langmuir isotherm, a graph of C_e/q_m against C_e was plotted, whereas, for the Freundlich model, a graph of $\ln q_e$ against $\ln C_e$ was

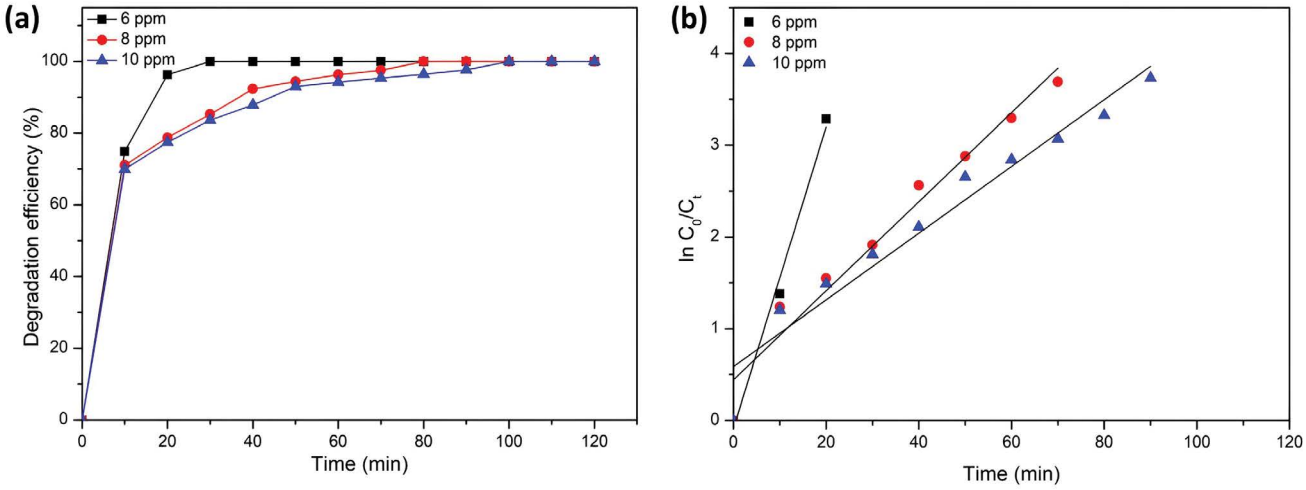

Fig. 7. (a) Degradation efficiency of neutral red under sunlight irradiation with an initial dye concentration of 6, 8 and 10 ppm and (b) first-order linear transform $\ln(C_0/C_t)$ of neutral red degradation plots against time for different initial dye concentrations of neutral red with 6, 8 and 10 ppm.

Table 2
Rate constants and correlation coefficients of degradation of neutral red under sunlight with concentrations

Initial concentration of neutral red (ppm)	Rate constant, k (min^{-1})	R^2
6	0.1643	0.9831
8	0.0458	0.9580
10	0.0364	0.9433

plotted. The result shows the correlative coefficient (R^2) of the Langmuir isotherm was higher (0.9920) when compared to the Freundlich isotherm (0.9731). Thus, the adsorption of NR by TiO_2 NPs tends to follow the Langmuir isotherm model. A higher value of R for the Langmuir model indicates that the adsorption process mathematically fits well. Since this experiment fitted well with the Langmuir model, it is assumed that the reaction was homogenous. The homogenous reaction by Langmuir adsorption isotherms is based on the assumption that the active sites are homogeneously distributed over the particulate's surface [16].

Favorable or unfavorable adsorption isotherm can be determined through the shape of the isotherm. The R_L value can be used to indicate whether the isotherm is favorable ($0 < R_L < 1$), unfavorable ($R_L > 1$), linear ($R_L = 1$) or irreversible ($R_L = 0$). R_L value can be calculated from Eq. (4):

$$R_L = \frac{1}{1 + bC_e} \tag{4}$$

Using Eq. (4) the value of R_L obtained was 0.432, indicating that the adsorption is favorable since the R_L value is within the range of 0 to 1.0. Hence, the synergistic effect of adsorption and photocatalysis is crucial that can effectively help to improve the photocatalytic performance of the photocatalyst in treating dye from the wastewater [49].

3.7. Mineralization study

The degree of mineralization for neutral red treated with the synthesized sample was determined using a TOC analyzer. TOC was based on the formation of CO_2 and other inorganic ions which were then converted to TOC or total carbon content. It was conducted to identify the total concentration of organics in the solution and the decrease of TOC reflects the degree of mineralization [50]. TOC removal of 89.21% was observed within 30 min. It can be deduced that the neutral red experienced nearly complete mineralization into CO_2 and H_2O with some intermediate products degraded during the process [22]. However, the result of TOC removal was relatively low compared to the degradation study determined by UV-Vis absorption spectroscopy since the percentage degradation of NR observed by this method within 30 min was 100% with the solution's color shifted from red to colorless. This phenomenon implies that only intermediate products are generated with no complete degradation of CO_2 occurring [22]. This result was in good agreement with Qian et al. [50] whereby they discovered that the TOC result (90%) was lower than the degradation efficiency of Acid red 3R dye (95%) by employing Aurum (Au) @ carbon (C)-TiO_{2-X} as a photocatalyst in their study. In our work, the intermediate degradation products are expected to be photo-oxidized to smaller molecules if the irradiation time is longer than 30 min, allowing for further conversion to CO_2 [51]. Hence, it may be concluded that the photocatalytic degradation of NR proceeds more rapidly than the decrease in TOC.

3.8. Scavenging study

In order to examine the potential reaction pathways during the photocatalytic degradation of NR dye under sunlight irradiation, a scavenging test was carried out to investigate the reactive oxygen species involved in this reaction. Reactive oxygen species (ROS) are those species

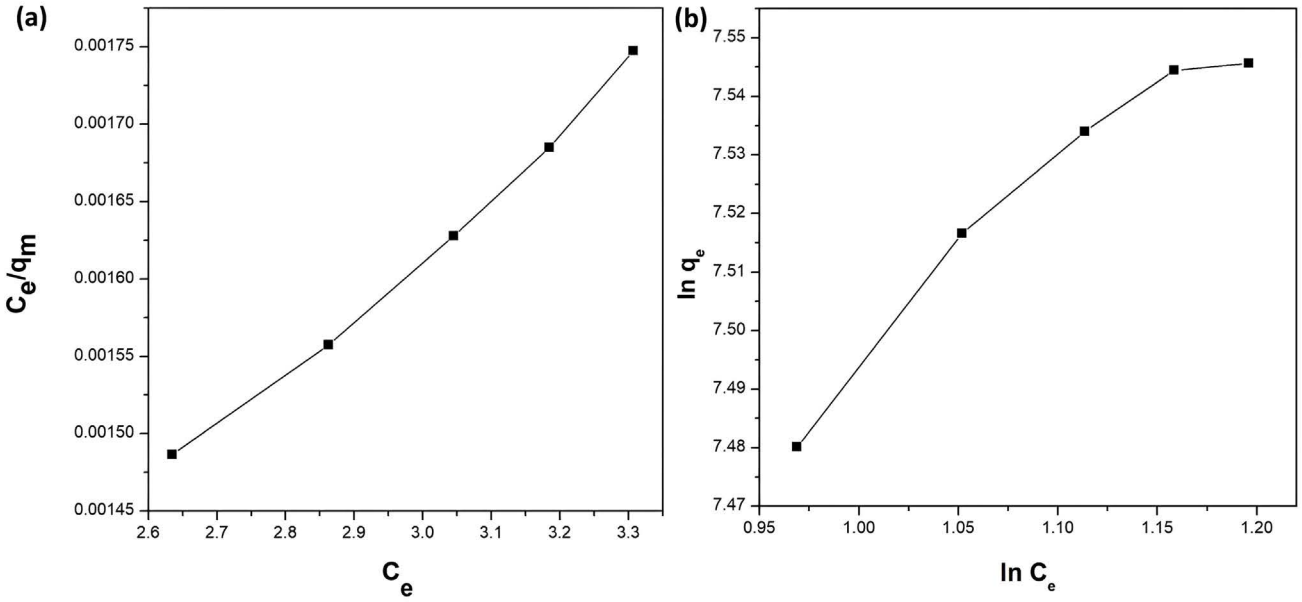

Fig. 8. (a) Langmuir isotherm showing the variation of adsorption (C_e/q_m) against the equilibrium concentration (C_e) for adsorption of TiO_2 NPs and (b) Freundlich isotherm showing the variation of adsorption ($\ln q_e$) against the equilibrium concentration ($\ln C_e$) for adsorption of TiO_2 NPs.

in which oxygen transforms with a high degree of reactivity [52]. The superoxide radicals ($^{\bullet}O_2^-$), hydroxyl radical ($^{\bullet}OH$), photogenerated holes (h^+), hydrogen peroxide (H_2O_2) as well as singlet oxygen ($^1O_2$) are recognized as among the primary ROS in the photocatalysis process [52]. Fig. 9 illustrates the free radical scavenging in the photodegradation of NR. Therefore, methanol (MeOH), silver nitrate ($AgNO_3$), acetonitrile (ACN), sodium pyruvate ($C_3H_3NaO_3$) and ascorbic acid ($C_6H_8O_6$) were used as scavengers for the photogenerated holes (h^+), superoxide radicals ($^{\bullet}O_2^-$), hydroxyl radicals ($^{\bullet}OH$), hydrogen peroxide (H_2O_2) and singlet oxygen ($^1O_2$), respectively. The result shows the rate of photodegradation of NR was found to be reduced when MeOH, $AgNO_3$, ACN, $C_3H_3NaO_3$, and $C_6H_8O_6$ were added compared to the initial activity before the scavengers were introduced. However, the use of $AgNO_3$ exhibited the strongest inhibition as it showed the greatest reduction which is 72.05% removal of NR followed by $C_6H_8O_6$ (80.16%), $C_3H_3NaO_3$ (80.21%), ACN (80.30%) and MeOH (81.40%). Thus, this observation implies that $^{\bullet}O_2^-$ is the most active species and plays a prominent role in photocatalytic activity. Furthermore, methylene blue which was employed as the model pollutant in this study was known as a photosensitizer. Once the dye was exposed to the sunlight, it would promote the $^{\bullet}O_2^-$ generation with longer lifetimes, enhancing the photocatalytic activity of methylene blue [53].

3.9. Proposed mechanism of neutral red degradation

In this study, the scavenging result observed that the $^{\bullet}O_2^-$ plays a prominent role in the photodegradation of NR followed by $^1O_2$, H_2O_2, $^{\bullet}OH$ and h^+. Therefore, an essential mechanism in the degradation of NR can be proposed. First,

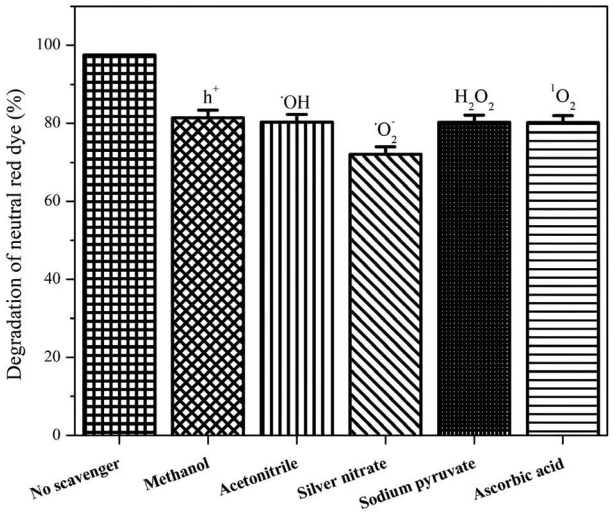

Fig. 9. Radical scavenging test of the TiO_2 photocatalyst using methanol, acetonitrile, silver nitrate, sodium pyruvate and ascorbic acid (n = 3).

photoexcited electrons are promoted from the valence band (VB) to the conduction band (CB), forming an electron/hole pair (e^-/h^+) in the photocatalytic reaction of TiO_2 in Eq. (5). Next, the reduction of adsorbed O_2 to $^{\bullet}O_2^-$ in the conduction band electron is important since $^{\bullet}O_2^-$ shows a dominant role in Eq. (6). Then, the production of $^{\bullet}O_2^-$ will degrade NR molecules into harmless products such as CO_2 and water in Eq. (7) [16,22]. Moreover, these $^{\bullet}O_2^-$ ions can react with hydrogen ions in the solution forming H_2O_2 and producing hydroxyl radicals ($^{\bullet}OH$), which are responsible for the degradation of NR in Eqs. (8) and (9). Besides, the photogenerated holes (h^+)

were also reported to produce hydroxyl radicals (•OH) which are responsible for the degradation of NR compounds into harmless chemicals in Eqs. (10) and (11) [16]. Furthermore, singlet oxygen ($^1O_2$) species are created by the reaction of h^+ with $•O_2^-$, whereby subsequently degrade NR in Eq. (12) [49]. Hence, this observation demonstrated that the degradation of NR into CO_2 and H_2O is attributed to the generation of singlet oxygen ($^1O_2$), hydrogen peroxide (H_2O_2), superoxide radicals ($•O_2^-$), photogenerated holes (h^+), and hydroxyl radical (•OH) with a dominant role is played by $•O_2^-$. The possible pathway for NR degradation is illustrated with Eq. (5) until (12) and Fig. 10 is expressed:

$$TiO_2 + hv \rightarrow e^-_{CB} + h^+_{VB} \quad (5)$$

$$O_2 + e^-_{CB} \rightarrow •O_2^- \quad (6)$$

$$•O_2^- + NR \rightarrow CO_2 + H_2O \quad (7)$$

$$•O_2^- + 2H^+ \rightarrow H_2O_2 \quad (8)$$

$$H_2O_2 + hv \rightarrow 2OH• + NR \rightarrow CO_2 + H_2O \quad (9)$$

$$h^+_{VB} + H_2O \rightarrow •OH + H^+ \quad (10)$$

$$•OH + NR \rightarrow CO_2 + H_2O \quad (11)$$

$$h^+_{VB} + •O_2^- \rightarrow {}^1O_2 + NR \rightarrow CO_2 + H_2O \quad (12)$$

3.10. Reusability of the TiO_2 NPs photocatalyst

To evaluate the feasibility of repeated use of TiO_2 photocatalyst, five cycles of photocatalytic degradation of NR were carried out in duplicates. The result shows the degrading efficiency of NR reduced by just around 9.96% from 100% to 90.04% after five cycles as depicted in Fig. 11. The average removal of NR in the first cycle was 97.51%, implying that NR removal efficiency dropped by only about 2% over this cycle. Hence, the TiO_2 photocatalysts showed good stability throughout the photocatalytic degradation of NR under sunlight irradiation since there is no noticeable loss in photocatalytic activity after five recycling tests. This very small decrease is probably due to the reused photocatalyst's adsorption capacity and active sites have decreased [48]. Moreover, the decline in the degrading efficiency might be caused by material loss during the washing and filtration process [15]. However, the reusability confirms the excellent stability of TiO_2 NPs in powder form which can provide a good photocatalytic activity.

4. Conclusion

In this research, the green synthesis of a sol–gel method was successfully applied to synthesize TiO_2 NPs by employing titanium isopropoxide (TTIP) as a titanium precursor. The obtained TiO_2 NPs have the optical bandgap of 3.00 eV, which has been reduced from 3.20 eV of pure anatase TiO_2.

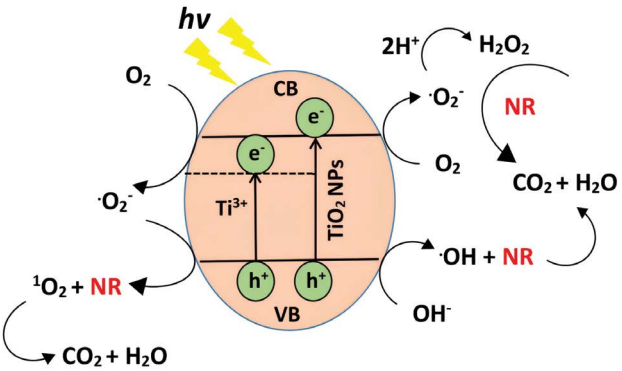

Fig. 10. Schematic diagram of the proposed degradation mechanism of neutral red dye under visible light irradiation.

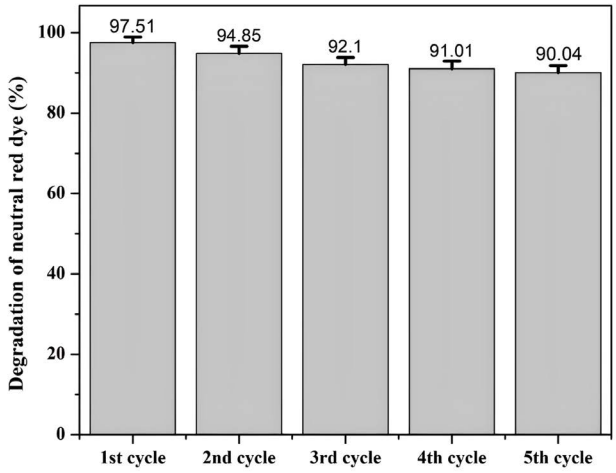

Fig. 11. Reusability test of synthesized TiO_2 nanoparticles (n = 3).

However, the resultant EC bandgap of 2.81 eV was an insignificant difference compared to the optical bandgap based on the student's t-test. The PL analysis indicated that synthesized TiO_2 has low intensity compared to the pure anatase TiO_2 conforming to the slower recombination rate of photo-induced electron–hole pairs. Besides, the XRD analysis demonstrated the presence of the anatase-brookite mixture phase of TiO_2 NPs with a crystallite size of 8 nm. This finding is in good agreement with HRTEM analysis, showing irregular spherical particles with an average size of 11.63 ± 1.47 nm. Next, the TiO_2 NPs were successfully used as a photocatalyst in the photocatalytic degradation of NR dye. The optimal initial dye concentration obtained for the degradation of NR solution under sunlight is 6 ppm. The degradation of NR at optimal dye concentration was found to follow first-order kinetics with k = 0.1643 min^{-1}. Meanwhile, the adsorption isotherm analysis was best fitted with the Langmuir isotherm model, indicating the reaction was homogenous. Mineralization study by TOC gives the removal of 89.21% within 30 min suggesting the mineralization rate is slower compared to the degradation rate since only intermediate products are generated with no complete degradation to CO_2 occurring. The scavenging

test in photodegradation of NR revealed that the $^{\bullet}O_2^-$ is the main active ROS that played the dominant role in the photocatalytic activity. The reusability study revealed that TiO_2 NPs could be reused for up to five cycles under sunlight irradiation with the degradation efficiency of NR at 90.04%. In short, TiO_2 NPs synthesized by a sol–gel method have shown to be an effective photocatalyst for the degradation of NR under sunlight irradiation and a promising candidate for photocatalysis application in wastewater treatment.

Symbols

C_0	—	Initial concentration of NR, ppm
C_t	—	Concentration of the NR at respective time intervals (t), ppm
C_e	—	Equilibrium concentration of NR, ppm
τ	—	Average crystallite size of the solid particle, nm
K	—	Scherrer constant, 0.9
λ	—	X-ray wavelength, 0.154 nm
β	—	Full width at half maximum intensity, FWHM
E_{pa}	—	Anodic peak potential, V
E_{pc}	—	Cathodic peak potential, V
R_L	—	Separation factor
R^2	—	Linear regression coefficient
q_m	—	Maximum adsorption capacity, mg/g
q_e	—	Adsorption capacity at equilibrium, mg/g
hv	—	Sunlight irradiation
TiO_2	—	Titanium dioxide
e^-_{CB}	—	Electron at conduction band
h^+_{VB}	—	Hole at valence band
$^{\bullet}O_2^-$	—	Superoxide radical
h^+	—	Hydrogen ion
H_2O_2	—	Hydrogen peroxide
$^{\bullet}OH$	—	Hydroxyl radical
$^1O_2$	—	Singlet oxygen
O_2	—	Oxygen
CO_2	—	Carbon dioxide
H_2O	—	Water
NR	—	Neutral red dye

Acknowledgements

The authors wish to thank the Ministry of Higher Education (MOHE) Malaysia for the Fundamental Research Grant Scheme with Project Code: FRGS/1/2019/STG07/USM/02/17.

Conflict of interest

The authors declare that they have no known competing financial interests or personal relationships that could have appeared to influence the work reported in this paper.

References

[1] M. Rauf, S. Ashraf, Fundamental principles and application of heterogeneous photocatalytic degradation of dyes in solution, Chem. Eng. J., 151 (2009) 10–18.
[2] L. Lin, W. Jiang, L. Chen, P. Xu, H. Wang, Treatment of produced water with photocatalysis: recent advances, affecting factors and future research prospects, Catalysts, 10 (2020) 924, doi: 10.3390/catal10080924.
[3] J. Conkle, C. Lattao, J. White, R. Cook, Competitive sorption and desorption behavior for three fluoroquinolone antibiotics in a wastewater treatment wetland soil, Chemosphere, 80 (2010) 1353–1359.
[4] J. Gregory, R. Dhond, Wastewater treatment by ion exchange, Water Res., 6 (1972) 681–684.
[5] S. Hube, M. Eskafi, K. Hrafnkelsdóttir, B. Bjarnadóttir, M. Bjarnadóttir, S. Axelsdóttir, B. Wu, Direct membrane filtration for wastewater treatment and resource recovery: a review, Sci. Total Environ., 710 (2020) 136375, doi: 10.1016/j.scitotenv.2019.136375.
[6] F.D. Guerra, M.F. Attia, D.C. Whitehead, F. Alexis, Nanotechnology for environmental remediation: materials and applications, Molecules, 23 (2018) 1760, doi: 10.3390/molecules23071760.
[7] S. Horikoshi, N. Serpone, Can the photocatalyst TiO_2 be incorporated into a wastewater treatment method? background and prospects, Catal. Today, 340 (2020) 334–346.
[8] M.M. Byranvand, A.N. Kharat, L. Fatholahi, Z.M. Beiranvand, A review on synthesis of nano-TiO_2 via different methods, J. Nanostruct., 3 (2013) 1–9.
[9] L. Stephen, Titanium Dioxide Versatile Solid Crystalline: An Overview, In: R.S. Dongre, D.R. Peshwe, Eds., Assorted Dimensional Reconfigurable Materials, InTechOpen, London, United Kingdom, 2020.
[10] S.-Y. Lee, S.-J. Park, TiO_2 photocatalyst for water treatment applications, J. Ind. Eng. Chem., 19 (2013) 1761–1769.
[11] S. Valencia, J. Marín, G. Restrepo, Study of the bandgap of synthesized titanium dioxide nanoparticles using the sol–gel method and a hydrothermal treatment, Open Mater. Sci. J., 4 (2010) 9–14.
[12] J. Cui, F. Zhang, H. Li, J. Cui, Y. Ren, X. Yu, Recent progress in biochar-based photocatalysts for wastewater treatment: synthesis, mechanisms, and applications, Appl. Sci., 10 (2020) 1019, doi: 10.3390/app10031019.
[13] F. Paquin, J. Rivnay, A. Salleo, N. Stingelin, C. Silva-Acuña, Multi-phase microstructures drive exciton dissociation in neat semicrystalline polymeric semiconductors, J. Mater. Chem. C, 3 (2015) 10715–10722.
[14] X. Kang, S. Liu, Z. Dai, Y. He, X. Song, Z. Tan, Titanium dioxide: from engineering to applications, Catalysts, 9 (2019) 191, doi: 10.3390/catal9020191.
[15] S.S. Muniandy, N.H. Mohd Kaus, Z.-T. Jiang, M. Altarawneh, H.L. Lee, Green synthesis of mesoporous anatase TiO_2 nanoparticles and their photocatalytic activities, RSC Adv., 7 (2017) 48083–48094.
[16] N.H.M. Idris, J. Rajakumar, K.Y. Cheong, B.J. Kennedy, T. Ohno, A. Yamakata, H.L. Lee, Titanium dioxide/polyvinyl alcohol/cork nanocomposite: a floating photocatalyst for the degradation of methylene blue under irradiation of a visible light source, ACS Omega, 6 (2021) 14493–14503.
[17] H. Yang, K. Zhang, R. Shi, X. Li, X. Dong, Y. Yu, Sol–gel synthesis of TiO_2 nanoparticles and photocatalytic degradation of methyl orange in aqueous TiO_2 suspensions, J. Alloys Compd., 413 (2006) 302–306.
[18] N. Chaibakhsh, N. Ahmadi, M.A. Zanjanchi, Optimization of photocatalytic degradation of neutral red dye using TiO_2 nanocatalyst via Box–Behnken design, Desal. Water Treat., 57 (2016) 9296–9306.
[19] A.R. Johnsen, L.Y. Wick, H. Harms, Principles of microbial PAH-degradation in soil, Environ. Pollut., 133 (2005) 71–84.
[20] B. Pare, P. Singh, S. Jonnalagadda, Visible light-driven photocatalytic degradation and mineralization of neutral red dye in a slurry photoreactor, Indian J. Chem., 17 (2010) 391–395.
[21] M. Iram, C. Guo, Y. Guan, A. Ishfaq, H. Liu, Adsorption and magnetic removal of neutral red dye from aqueous solution using Fe_3O_4 hollow nanospheres, J. Hazard. Mater., 181 (2010) 1039–1050.
[22] B. Sarwan, B. Pare, A.D. Acharya, S.B. Jonnalagadda, Mineralization and toxicity reduction of textile dye neutral red in aqueous phase using BiOCl photocatalysis, J. Photochem. Photobiol., B, 116 (2012) 48–55.

[23] M.M. Alnuaimi, M.A. Rauf, S.S. Ashraf, Comparative decoloration study of neutral red by different oxidative processes, Dyes Pigm., 72 (2007) 367–371.
[24] X.-Z. Ding, Z.-Z. Qi, Y.-Z. He, Effect of hydrolysis water on the preparation of nano-crystalline titania powders via a sol–gel process, J. Mater. Sci. Lett., 14 (1995) 21–22.
[25] Y. Fang, J. Fu, P. Liu, B. Cu, Morphology and characteristics of 3D nanonetwork porous starch-based nanomaterial via a simple sacrifice template approach for clove essential oil encapsulation, Ind. Crops Prod., 143 (2020) 111939, doi: 10.1016/j.indcrop.2019.111939.
[26] M.M. Ahmad, S. Mushtaq, H. Al Qahtani, A. Sedky, M. Alam, Investigation of TiO_2 nanoparticles synthesized by sol–gel method for effectual photodegradation, oxidation and reduction reaction, Crystals, 11 (2021) 1456, doi: 10.3390/cryst11121456.
[27] S. Abbad, K. Guergouri, S. Gazaout, S. Djebabra, A. Zertal, R. Barille, M. Zaabat, Effect of silver doping on the photocatalytic activity of TiO_2 nanopowders synthesized by the sol–gel route, J. Environ. Chem. Eng., 8 (2020) 103718, doi: 10.1016/j.jece.2020.103718.
[28] D. Komaraiah, E. Radha, N. Kalarikkal, J. Sivakumar, M.V. Ramana Reddy, R. Sayanna, Structural, optical and photoluminescence studies of sol–gel synthesized pure and iron doped TiO_2 photocatalysts, Ceram. Int., 45 (2019) 25060–25068.
[29] Y. Quintero, E. Mosquera, J. Diosa, A. García, Ultrasonic-assisted sol–gel synthesis of TiO_2 nanostructures: influence of synthesis parameters on morphology, crystallinity, and photocatalytic performance, J. Sol-Gel Sci. Technol., 94 (2020) 477–485.
[30] X. Chen, S. Mao, Titanium dioxide nanomaterials: synthesis, properties, modifications, and applications, Chem. Rev., 107 (2007) 2891–2959.
[31] H.-J. Park, J.Y. Kim, J. Kim, J.-H. Lee, J.-S. Hahn, M.B. Gu, J. Yoon, Silver-ion-mediated reactive oxygen species generation affecting bactericidal activity, Water Res., 43 (2009) 1027–1032.
[32] G.L. Newton, J.R. Milligan, Fluorescence detection of hydroxyl radicals, Radiat. Phys. Chem., 75 (2006) 473–478.
[33] K. Kawasaki, Y. Kamagata, Phosphate-catalyzed hydrogen peroxide formation from agar, gellan, and κ-carrageenan and recovery of microbial cultivability via catalase and pyruvate, Appl. Environ. Microbiol., 83 (2017) e01366, doi: 10.1128/AEM.01366-17.
[34] M.A. Ahmed, E.E. El-Katori, Z.H. Gharni, Photocatalytic degradation of methylene blue dye using Fe_2O_3/TiO_2 nanoparticles prepared by sol–gel method, J. Alloys Compd., 553 (2013) 19–29.
[35] S.L.N. Zulmajdi, N.I.I. Zamri, A.H. Mahadi, M.Y.H. Rosli, F. Ja'afar, H.M. Yasin, E. Kusrini, J. Hobley, A. Usman, Sol–gel preparation of different crystalline phases of TiO_2 nanoparticles for photocatalytic degradation of methylene blue in aqueous solution, Am. J. Nanomater., 7 (2019) 39–45.
[36] B.H. Toby, R factors in Rietveld analysis: how good is good enough?, Powder Diffr., 21 (2006) 67–70.
[37] N.S. Allen, N. Mahdjoub, V. Vishnyakov, P.J. Kelly, R.J. Kriek, The effect of crystalline phase (anatase, brookite and rutile) and size on the photocatalytic activity of calcined polymorphic titanium dioxide (TiO_2), Polym. Degrad. Stab., 150 (2018) 31–36.
[38] T.A. Kandiel, L. Robben, A. Alkaim, D. Bahnemann, Brookite versus anatase TiO_2 photocatalysts: phase transformations and photocatalytic activities, Photochem. Photobiol. Sci., 12 (2013) 602–609.
[39] W. Nachit, H. Ait Ahsaine, Z. Ramzi, S. Touhtouh, I. Goncharova, K. Benkhouja, Photocatalytic activity of anatase-brookite TiO_2 nanoparticles synthesized by sol–gel method at low temperature, Opt. Mater. (Amst.), 129 (2022) 112256, doi: 10.1016/j.optmat.2022.112256.
[40] K.V. Baiju, S. Shukla, K.S. Sandhya, J. James, K.G.K. Warrier, Photocatalytic activity of sol–gel-derived nanocrystalline titania, J. Phys. Chem. C, 111 (2007) 7612–7622.
[41] M.C. Ceballos-Chuc, C.M. Ramos-Castillo, M. Rodríguez-Pérez, M.Á. Ruiz-Gómez, G. Rodríguez-Gattorno, J. Villanueva-Cab, Synergistic correlation in the colloidal properties of TiO_2 nanoparticles and its impact on the photocatalytic activity, Inorganics, 10 (2022) 125, doi: 10.3390/inorganics10090125.
[42] D. Li, H. Song, X. Meng, T. Shen, J. Sun, W. Han, X. Wang, Effects of particle size on the structure and photocatalytic performance by alkali-treated TiO_2, J. Nanomater., 10 (2020) 546, doi: 10.3390/nano10030546.
[43] S.K. Haram, B.M. Quinn, A.J. Bard, Electrochemistry of CdS nanoparticles: a correlation between optical and electrochemical bandgaps, J. Am. Chem. Soc., 123 (2001) 8860–8861.
[44] R. Fernández-Climent, S. Giménez, M. García-Tecedor, The role of oxygen vacancies in water splitting photoanodes, Sustainable Energy Fuels, 4 (2020) 5916–5926.
[45] B. Plešngerová, G. Sučik, M. Maryška, D. Horkavcova, Hydroxyapatite coatings deposited from alcohol suspensions by electrophoretic deposition on titanium substrate, Ceram. Silik., 51 (2007) 15–23.
[46] K. Kato, Y. Uemura, K. Asakura, A. Yamakata, Role of oxygen vacancy in the photocarrier dynamics of WO_3 photocatalysts: the case of recombination centers, J. Phys. Chem. C, 126 (2022) 9257–9263.
[47] N. Ali, A. Said, F. Ali, F. Raziq, Z. Ali, M. Bilal, L. Reinert, T. Begum, H.M.N. Iqbal, Photocatalytic degradation of Congo red dye from aqueous environment using cobalt ferrite nanostructures: development, characterization, and photocatalytic performance, Water Air Soil Pollut., 231 (2020) 50, doi: 10.1007/s11270-020-4410-8.
[48] M.F. Hanafi, N. Sapawe, Effect of initial concentration on the photocatalytic degradation of Remazol Brilliant Blue dye using nickel catalyst, Mater. Today Proc., 31 (2020) 318–320.
[49] J. Chen, Y. Xiong, M. Duan, X. Li, S. Fang, S. Qin, R. Zhang, Insight into the synergistic effect of adsorption–photocatalysis for the removal of organic dye pollutants by Cr-doped ZnO, Langmuir, 36 (2020) 520–533.
[50] H. Qian, Q. Hou, E. Duan, J. Niu, Y. Nie, C. Bai, X. Bai, M. Ju, Honeycombed Au@C-TiO_{2-X} catalysts for enhanced photocatalytic mineralization of Acid red 3R under visible light, J. Hazard. Mater., 391 (2020) 122246, doi: 10.1016/j.jhazmat.2020.122246.
[51] B. Ghasemi, B. Anvaripour, S. Jorfi, N. Jaafarzadeh, Enhanced photocatalytic degradation and mineralization of furfural using UVC/TiO_2/GAC composite in aqueous solution, Int. J. Photoenergy, 2016 (2016) 2782607, doi: 10.1155/2016/2782607.
[52] J. Rodrigues, T. Hatami, J.M. Rosa, E.B. Tambourgi, Photocatalytic degradation of Reactive Blue 21 dye using ZnO nanoparticles: experiment, modelling, and sensitivity analysis, Environ. Technol., 42 (2021) 3675–3687.
[53] I.D. Rettig, T.M. McCormick, Enrolling reactive oxygen species in photon-to-chemical energy conversion: fundamentals, technological advances, and applications, Adv. Phys.: X, 6 (2021) 1950049, doi: 10.1080/23746149.2021.1950049.